J Mater Sci: Mater Electron (2016) 27:2830–2835
DOI 10.1007/s10854-015-4097-6

Magnetic properties of structure ordered cores composited with $Fe_{78}Si_9B_{13}$ amorphous and pure iron powders

Y. Y. Zheng[1] · Y. G. Wang[1]

Received: 28 August 2015 / Accepted: 16 November 2015 / Published online: 23 November 2015

Abstract Composite cores of $Fe_{78}Si_9B_{13}$ amorphous and pure iron powder were prepared by cold pressing. Effective permeability, initial permeability and the magnetic flux density of cores can all be improved by increasing the content of pure iron powder. With and without an external magnetic field, the circularly orientated (COCPC) and non-oriented (NOCPC) composite powder cores were obtained. The effect of the shape anisotropy of the flake powders on magnetic properties of the composite powder cores was investigated. All investigated magnetic properties of COCPC cores are better than those of NOCPC cores with the same mixture ratio and the effect of structural ordering weakens as the content of pure iron powder increases. For cores with only amorphous powder the effective permeability below 100 kHz, the initial permeability and the magnetic flux density for $H_{max} = 8$ kA m^{-1} of COCPC increase by 8.1, 15 and 10 %, respectively, compared to those of the NOCPC. Pressing magnetic powders under an external magnetic field to form ordered structure is suitable for optimal design of soft magnetic cores toward practical applications.

1 Introduction

The soft magnetic materials of powder cores such as Fe-based amorphous powders prepared by crushing ribbons have been widely used as electromagnetic components to meet the specialized requirements for practical applications [1–4]. In recent years, various factors affecting the magnetic powder core have been verified [5–8] and the potential for performance improvement is small in view of a single powder. Compositing two kinds of powder is expected to be a hopeful way to achieve excellent magnetic properties of cores [9–13]. Kim [10] found that the amorphous powder mixed with pure iron powder improved compactability of powder, which resulted in the increase of the density and permeability of powder cores. However, the influence of the shape anisotropy of powders on the magnetic properties of the composite powder cores has not been considered. The properties of magnetic materials depend strongly on their shapes and applying an external magnetic field in preparing oriented composites is proved to be an effective method [14–17]. The powders will be orientated to form ordered structure along the magnetic lines under an external magnetic field and the flaky powders will lie parallel to each other to form a layered microstructure in the core which may be ideal for achieving the excellent magnetic properties of the cores [18]. In the present work the flake-type crushed $Fe_{78}Si_9B_{13}$ amorphous powder mixed with flake-type pure iron powder are orientated with an external magnetic field in the mold. The effect of the circular orientation on the magnetic properties of the composite powder core will be investigated. The flaky morphology of two kinds of powder used here is beneficial to maintaining a high degree of orientation in the process of pressing. The modified powder compaction process is expected to show a good potential for the advanced powder core with excellent magnetic properties.

2 Experimental

The amorphous powder was prepared by crushing $Fe_{78}Si_9B_{13}$ amorphous ribbons as the first magnetic powder, and the pure iron powder as the second magnetic powder.

✉ Y. G. Wang
yingang.wang@nuaa.edu.cn

[1] College of Materials Science and Technology, Nanjing University of Aeronautics and Astronautics, Nanjing 210016, People's Republic of China

$Fe_{78}Si_9B_{13}$ amorphous ribbons (width: 10–30 mm,thickness: 26–32 μm) were annealing at 533 K for 2 h in vacuum and then converted to flakes by ball-milling followed with jet-milling. The pure iron powder was used as raw materials and milled with calcium stearate and acetone in a planetary ball mill for 6 h (500 rpm) to form flaky iron powder. The sieved $Fe_{78}Si_9B_{13}$ amorphous powders with sizes of 50–150 μm (Fig. 1a) and the pure iron powders with sizes of 50–250 μm (Fig. 1b) were used to prepare the composite powder cores. The composite powders were passivated by phosphoric acid and uniformly mixed with 1.0 wt% of organic binders (methyl silicone) and 0.5 wt% of zinc stearate. The loose filled powder mixtures were then circularly orientated with an external magnetic field of 0.2 mT. The schematic diagram of orientation process is shown in Fig. 3a. Toroidal powder cores with non-oriented and circularly oriented structures were formed by using the press molding process under a compaction pressure of 800 MPa. The powder alignment before the modeling procedure is shown schematically in Fig. 3b and that in the circularly ordered cores is shown in Fig. 3c. All cores were finally annealed at 673 K in an argon atmosphere for 0.5 h. The obtained cores were with outer and internal diameters of 29.4 and 17.5 mm, and a height of about 10 mm, the physical figure of composite powder cores is shown in Fig. 3d. After forming, the composite powder cores were demagnetized. The mixing ratios of pure Fe powder to $Fe_{78}Si_9B_{13}$ amorphous powder were 0, 25, 50, 75 and 100 wt%, respectively. For convenience, the non-oriented composite powder cores, the oriented composite powder cores are named as NOCPC and COCPC, respectively.

The density (ρ) and the volume fraction (P) of the composite powder cores were measured by the Archimedes method. The structure of cores after annealing at 673 K was examined by X-ray diffractometry (XRD) with Cu-Kα and the amorphous state was confirmed as shown in Fig. 2. Scanning electron microscopy (SEM) images were obtained by using a FEI Quanta650 scanning electron microscope. The static magnetic properties for the samples were carried out at room temperature with a B–H loop tracer with the maximum magnetic field of 8 kA m^{-1}. The frequency dependence of the effective permeability (μ_e) was measured using an LCR meter (GWINSTEK 819 LCR).

3 Results and discussion

Figure 1 shows the morphology of the $Fe_{78}Si_9B_{13}$ crushed amorphous powders and the pure iron powders observed by SEM. One can see that these two kinds of powders are anisometric flakes with sharp edges and high ratios of diameter to thickness. Therefore, the static magnetic force is larger than the friction force between powders in a loose state under an external magnetic field and the induced magnetic dipole will aligned along the long axis of powders, and thus the powders will be orientated along the magnetic lines.

Figure 3b shows the possible stacking arrangements of square flakes in the COCPC. The long axis of powders is parallel to the external magnetic field in preparation and the flakes lie parallel to one another and separated by an insulating layer. One can see that there is no closed magnetic circuit and thus produces a demagnetizing field within the powders antiparallel to the external magnetic field.

The internal magnetic field H_i of the powders can be calculated from the following equation [19]:

$$H_i = H_e + H_d = H_e - NM \quad (1)$$

where H_e is the external magnetic field, H_d is the demagnetizing field, N is the demagnetization factor and M is the magnetization.

The effective permeability μ_e of the cores can be written as [19]

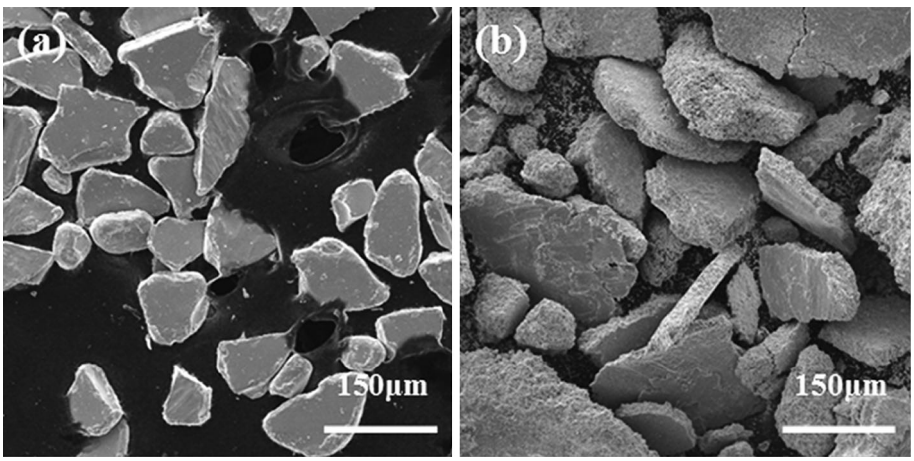

Fig. 1 Morphology of crushed $Fe_{78}Si_9B_{13}$ amorphous (**a**) and pure iron powders (**b**)

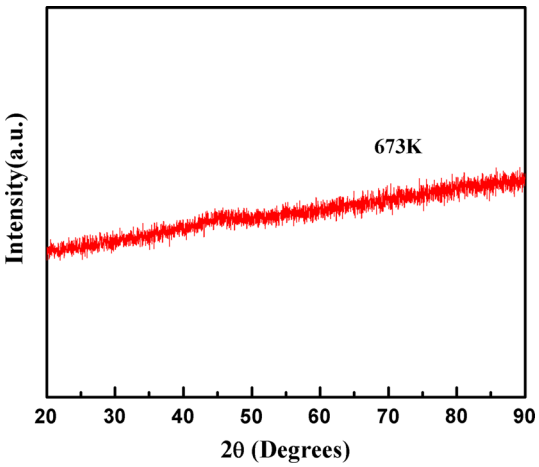

Fig. 2 XRD pattern of amorphous powder cores after annealing at 673 K

$$\mu_e = 1 + \frac{4\pi(\mu - 1)}{4\pi + N(\mu - 1)}p \tag{2}$$

where μ is the intrinsic permeability of the material and p is the total volume fraction of magnetic particles in the composites.

The effective permeability μ_e of composite cores depends on the permeability of the powders μ, the volume fraction p, and the demagnetizing factor N of the powders. Flake powders have a higher demagnetization factor in the thickness direction and a lower one in the long axis direction [20]. Therefore it is reasonable to expect that in cores with ordered powders the effective permeability is anisotropic and the cores show the highest permeability in the direction along the long axis of powders.

The type of orientation of COCPC has been illustrated schematically in Fig. 3c. Examples of the cross-sectional SEM images of the NOCPC and COCPC with 25, 50 and 75 wt% Fe are shown in Fig. 4. Flakes of pure iron powders have been broken and fill the gap positions between $Fe_{78}Si_9B_{13}$ amorphous powders. It can be seen from Fig. 4b, d, f that the NOCPC cores present a relatively disordered structure of flake powders, the edges of which lie against each other. The cross-section of COCPC cores present an ordered arrangement of powders and a layered structure and the powders lie parallel to one another separated by an insulating layer as shown in Fig. 4a, c, e. One can see that the movement of flake powders along the magnetic lines results in a regular planar orientation of the powders in these cores.

Figure 5 shows the density and the total volume fraction of magnetic powders as functions of the content of pure iron powder. The density of pure Fe powder (7.82 g cm^{-3}) is higher than that of amorphous $Fe_{78}Si_9B_{13}$ powder (7.18 g cm^{-3}). The mixtures with pure iron powder can improve the compactability of the $Fe_{78}Si_9B_{13}$ amorphous powder. The density ρ and volume fraction P can be increased by increasing the mixing ratio of pure iron powder in composite cores. Indeed, the density can be expressed following the rule of mixtures equation [9]:

$$\rho_{composite} = \sum_{1}^{N} \rho_i f_i \tag{3}$$

where ρ_i is the density of phase i, f_i is the volumetric fraction of phase i and N is the number of phases, which comprise the composite. One can also see that the values of

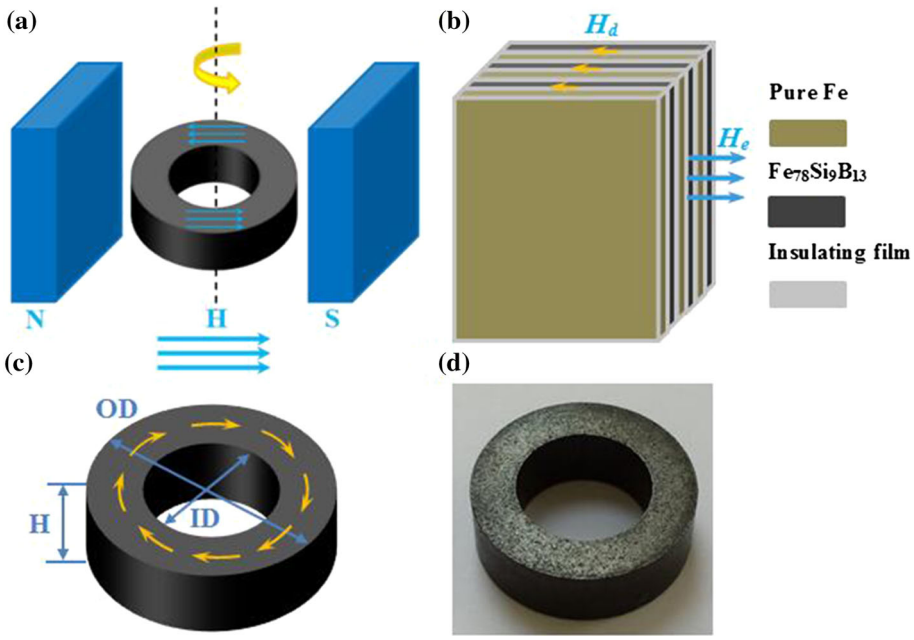

Fig. 3 **a** Schematic diagram of orientation process; **b** possible stacking pattern of powders in oriented composite cores; **c** schematic diagram of oriented composite powder cores; **d** physical figure of composite powder cores

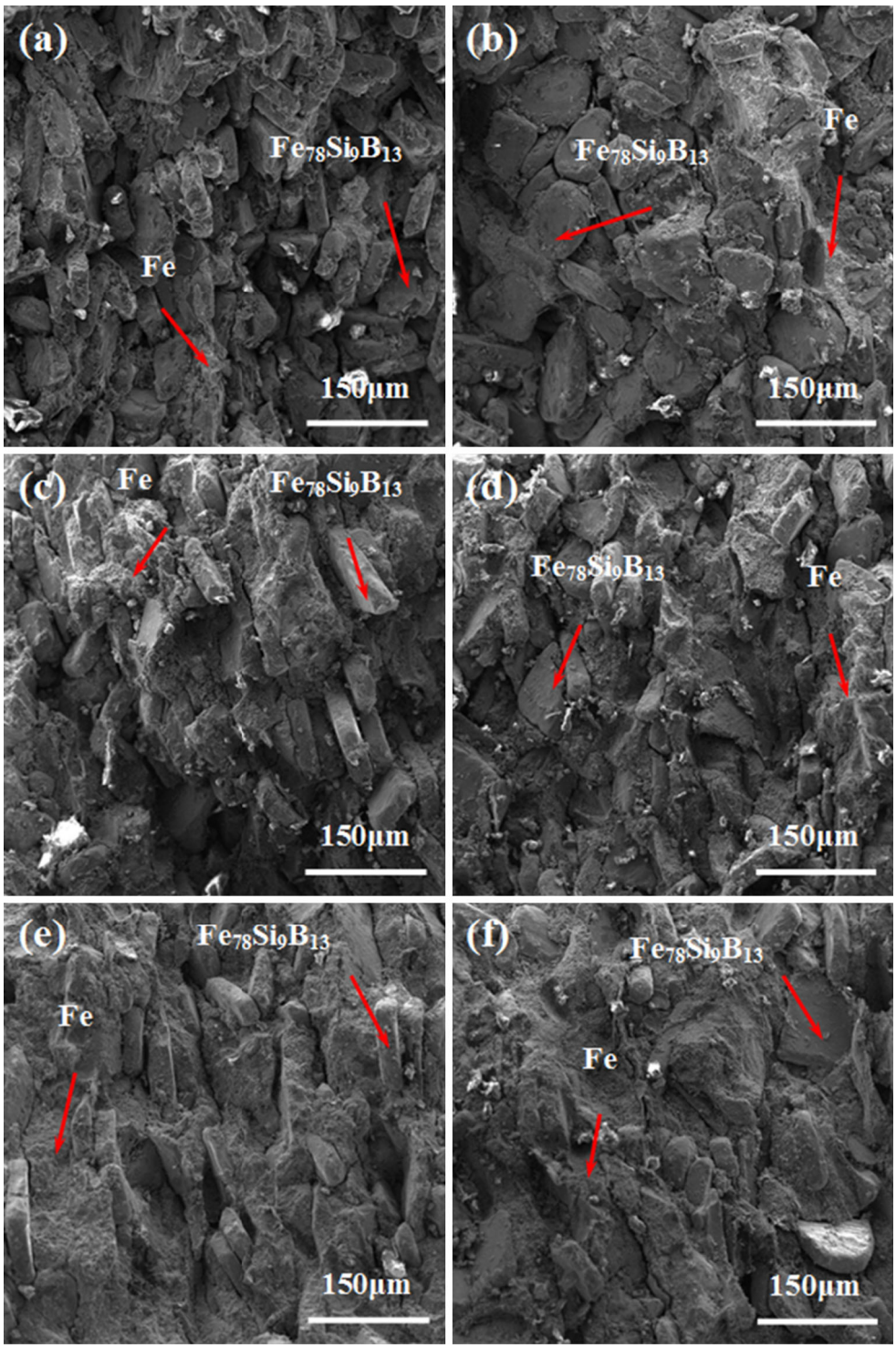

Fig. 4 Cross-sectional SEM images of composite powder cores: **a** COCPC (25 wt% Fe), **c** COCPC (50 wt% Fe) and **e** COCPC (75 wt% Fe); and **b** NOCPC (25 wt% Fe), **d** NOCPC (50 wt% Fe) and **f** NOCPC (75 wt% Fe)

these two physical properties of COCPC are higher than those of NOCPC with the same content of pure iron powder and as the content of pure iron powder increases the effect of structural ordering weakens. It is ascribed to the fact that the layered structure of COCPC is beneficial to obtain high density of composite powder cores. On the other hand, the stiffness of pure iron powders is relatively lower than the $Fe_{78}Si_9B_{13}$ amorphous powders and the flake-type pure iron powders were destroyed by compaction under 800 MPa as shown in Fig. 4, therefore, the effect of powders orientation on density will be weakened with the increase of pure iron powder content.

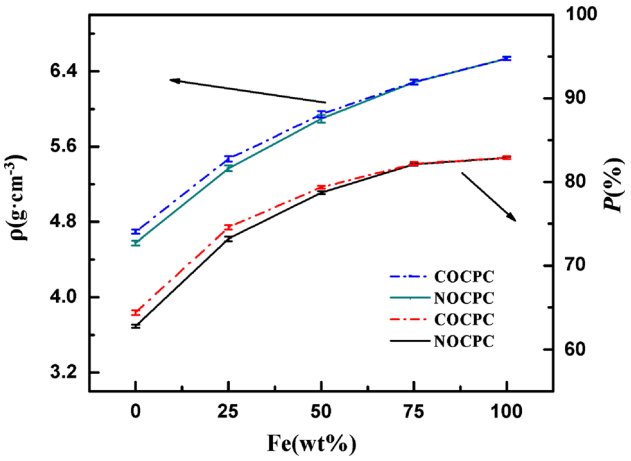

Fig. 5 Variation of density ρ and volume fraction P of the composite powder cores with the content of pure iron powder

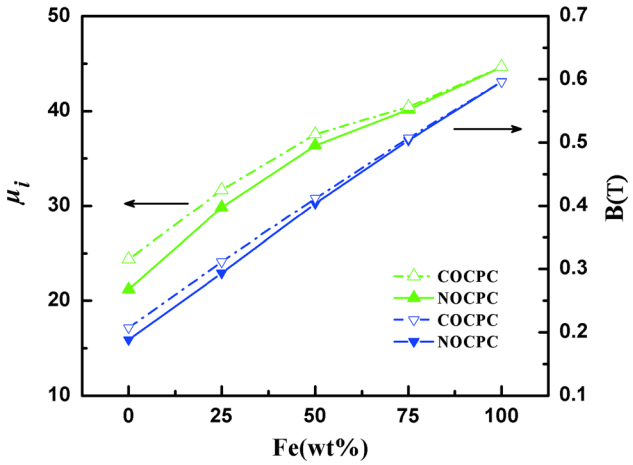

Fig. 7 Variations of μ_i and B of the composite powder cores with pure iron powder content in the mixed powders

Figure 6 shows the frequency dependences of the effective permeability (μ_e) of composite powder cores with various pure iron contents. It can be seen that the cores all show stable permeability below 100 kHz and the effective permeability tends to increase with the increasing percentage of pure iron powder. As expected the effective permeability of the COCPC is higher than that of the NOCPC with the same content of pure iron powder and as the content of pure iron powder increases the improvement weakens. For composite powder cores without pure Fe powder, the μ_e of COCPC improves 8.1 % compared to that of NOCPC. This result could be interpreted in two aspects. One is the reduction of air gaps caused by the ordered structure of powders which increases the amount of magnetic phases in unit volume. The other is the circular orientation structure of magnetic powders which reduce the demagnetization factor of the composite cores. The impact of these two factors will become weak with the increase of pure iron powder content.

Figure 7 depicts the initial permeability (μ_i), the magnetic flux density (B) as a function of the content of pure iron powder for $H_{max} = 8$ kA m^{-1}. The μ_i and B increase with the increasing of the content of pure iron powder, which results from the increased density of the cores by addition of pure iron powder [18, 21]. The μ_i and B of COCPC are higher than those of NOCPC with the same content of pure iron powder. As the content of pure iron powder increases the improvement of them also weakens, which can be attributed to the fact that, with the increase of pure iron powder content, the amplitude of density increasement becomes smaller. For composite powder cores without pure Fe powder, the μ_i and B for $H_{max} = 8$ kA m^{-1} of COCPC improve 15 and 10 %, respectively, compared to those of NOCPC.

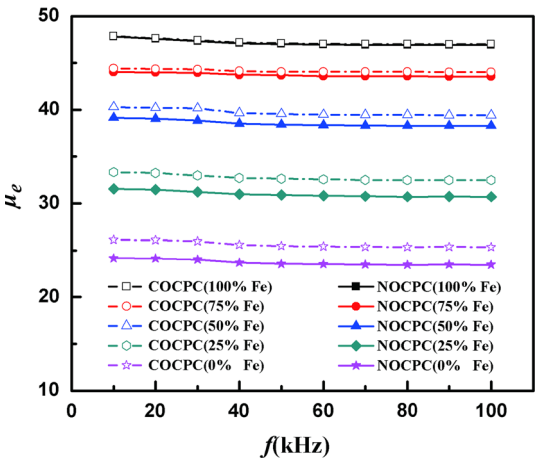

Fig. 6 Frequency dependences of the effective permeability of composite powder cores

4 Conclusions

Effects of the circular orientation of magnetic powders on magnetic properties of the composite cores were investigated. An external magnetic field is proved to be effective in improving magnetic properties due to the shape anisotropy of flake powders. Orientation parallel to the external magnetic field in preparation is the optimal one for powder cores and causes the improvement of soft magnetic properties. The density, volume fraction of magnetic phases, the effective permeability below 100 kHz, the initial permeability and the magnetic flux density for $H_{max} = 8$ kA m^{-1} can all be increased by increasing the mixing ratio of pure iron powder in composite cores. For cores with only amorphous powder the effective permeability below 100 kHz, the initial permeability and the magnetic flux

density for $H_{max} = 8$ kA m^{-1} of COCPC increase by 8.1, 15 and 10 %, respectively, compared to those of the NOCPC. The improvement of soft magnetic properties of ordered structures is helpful for optimal design of magnetic composite cores toward practical application.

Acknowledgments This work is supported by Natural Science Foundation of China (No. 51571115), Joint Innovation Foundation of Industry and University of Jiangsu Province (No. BY2013003-01) and a Project Funded by the Priority Academic Program Development of Jiangsu Higher Education Institutions.

References

1. X. Lia, A. Makino, H. Kato, A. Inoue, T. Kubot, Mater. Sci. Eng. B **176**, 1247 (2011)
2. J. Füzer, S. Dobák, P. Kollár, J. Alloys Compd. **628**, 335 (2015)
3. Y.P. Liu, Y.D. Yi, W. Shao, Y.F. Shao, J. Magn. Magn. Mater. **330**, 119 (2013)
4. J. Zhou, Y.F. Cui, H.S. Liu, W. Wang, K. Peng, Y.D. Xiao, J. Mater. Sci. **46**, 7567 (2011)
5. N.B. Dhokey, S. Patil, S. Dhandare, V.S. Bandal, Electron. Mater. Lett. **10**, 591 (2014)
6. R. Nowosielski, J.J. Wysłocki, I. Wnukb, P. Sakiewicz, P. Gramatyka, J. Mater. Process. Technol. **162**, 242 (2005)
7. I. Otsuka, T. Kadomura, K. Ishiyama, M. Yagi, IEEE Trans. Magn. **45**, 4294 (2009)
8. Y.B. Kim, D.H. Jang, H.K. Seok, K.Y. Kim, Mater. Sci. Eng. A **449**, 389 (2007)
9. E.A. Périgo, S. Nakahara, Y.P. Yamada, Y.D. Hazan, T. Graule, J. Magn. Magn. Mater. **323**, 1938 (2011)
10. H.J. Kim, S.K. Nam, K.S. Kim, S.C. Yoon, K.Y. Sohn, M.R. Kim, Y.S. Song, W.W. Park, J. Appl. Phys. **51**, 103001 (2012)
11. J. Füzerová, J. Füzer, P. Kollár, L. Hegedüs, R. Bureš, M. Fáberová, IEEE Trans. Magn. **48**, 1545 (2012)
12. X.Y. Wang, C.W. Lu, F. Guo, Z.C. Lu, D.R. Li, S.X. Zhou, J. Magn. Magn. **324**, 2727 (2012)
13. S.F. Chen, C.Y. Chen, C.S. Cheng, J. Alloys Compd. **644**, 17 (2015)
14. J.K. Lim, S.P. Yeap, C.H. Leow, P.Y. Toh, S.C. Low, J. Colloid Interface Sci. **421**, 170 (2014)
15. L.J. Zhao, H. Yang, L. Lu, J. Mater. Sci. Mater. Electron. **19**, 992 (2008)
16. R.P. Ji, J.S. Jiang, M. Hu, J. Phys. Chem. C **114**, 12090 (2010)
17. P. Saravanan, R. Gopalan, R. Priya, P. Ghosal, V. Chandrasekarana, J. Alloys Compd. **477**, 322 (2009)
18. Y. Zhang, P. Sharma, A. Makino, J. Appl. Phys. **115**, 17A322 (2014)
19. G.Q. Lin, Z.W. Li, L.F. Chen, Y.P. Wu, C.K. Ong, J. Magn. Magn. **305**, 291 (2006)
20. T. Liu, P.H. Zhou, L.J. Deng, W. Tang, J. Appl. Phys. **106**, 114904 (2009)
21. B.V. Neamtu, T.F. Marinca, I. Chicinas, O. Isnard, F. Popa, P. Păscută, J. Alloys Compd. **600**, 1 (2014)